SIMULATION AND MEASUREMENT OF FLOW PHENOMENA IN A COAXIAL JET MIXER

Nikolai Kornev, Igor Tkatchenko, Valery Zhdanov, Egon Hassel
Department of Technical Thermodynamics,
Steffen Jahnke
Department of Fluid Mechanics,
University of Rostock
Albert-Einstein-Str. 2, 18059 Rostock, Germany
nikolai.kornev@uni-rostock.de

ABSTRACT

Flow phenomena in a coaxial jet mixer are studied using numerical (LES) and experimental (LIF) methods. Measurements of distributions of a passive scalar (Rhodamin 6G) in mixer cross-sections at different distances from the nozzle have been carried out by Laser Induced Fluorescence (LIF) method. Distributions of the time averaged mixture fraction and its auto corellation functions across the mixer sections are presented. Calculations have been done with Large Eddy Simulation using an inflow generator and a clipping procedure proposed by the authors. The vortex structures are identified from the analysis based on the λ_2 criterion. Results for time averaged mixture fraction are compared with numerical results obtained by several LES and RANS models for the flow regime with the recirculation zone. The analysis revealed advantages of the dynamical mixed SGS model (DMM) compared with other models. Influence of different parameters of the flow on mixing is investigated.

INTRODUCTION

Mixing, particularly mixing in co-flows has been a subject of investigations for a long time because of their practical applications in many engineering devices such as combustion chambers, injection systems, etc. The jet mixers (see Fig. 1) possess excellent mixing properties due to strong vortices that appear at the jet boundary as a result of the instability in the shear layer. In this paper the classical jet mixer consisting of a nozzle of diameter d positioned along the center line of a pipe of diameter D has been considered. From dimensional analysis it can be shown that the characteristics of coaxial jet mixers depend on the ratio of diameters D/d, the Reynolds number $Re_d = dU_d/\nu$ based on the nozzle parameters, the Schmidt number Sc, the flow rate ratio $\dot{V}_D/\dot{V}_d$ and the fluid density ratio ρ_D/ρ_d. In none isothermal case the Prandtl number Pr and the temperature ratio $(T_D - T_d)/T_D$ are additional parameters.

Two qualitatively different flows can be observed in jet mixers, depending on the flow rate ratio $\dot{V}_D/\dot{V}_d$ (see Burchilon and Curtet (1964) and Henzler (1978)). If $D/d < 1 + \dot{V}_D/\dot{V}_d$ the flow is similar to the free jet flow regime. When $D/d > 1 + \dot{V}_D/\dot{V}_d$ a strong flow separation at pipe walls results in the recirculation zone behind the nozzle.

The aim of the present work is to get a detailed information on physics of flow and dynamics of passive scalar in a developed turbulent flow of the jet mixers (Fig. 1) both by numerical (LES) and experimental (LIF) methods.

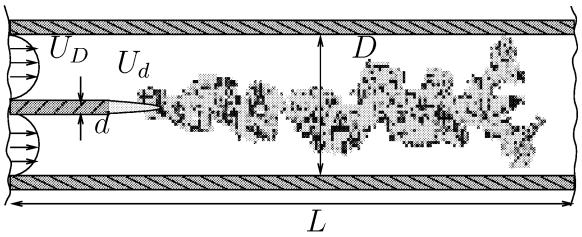

Figure 1: Scetch of a jet mixer

MATHEMATICAL MODEL

The LES equations are obtained by filtering the Navier-Stokes equation:

$$\frac{\partial \overline{u}_i}{\partial x_i} = 0, \tag{1}$$

$$\frac{\partial \overline{u}_i}{\partial t} + \frac{\partial \overline{u}_j \overline{u}_i}{\partial x_j} = \frac{1}{\rho}\frac{\partial}{\partial x_j}\left[\nu\left(\frac{\partial \overline{u}_i}{\partial x_j} + \frac{\partial \overline{u}_j}{\partial x_i}\right) + \tau_{ij}\right] - \frac{1}{\rho}\frac{\partial \overline{P}}{\partial x_i}, \tag{2}$$

$$\frac{\partial \overline{f}}{\partial t} + \frac{\partial \overline{u}_j \overline{f}}{\partial x_j} = -\frac{1}{\rho}\frac{\partial}{\partial x_j}\left[\frac{\nu}{Sc}\frac{\partial \overline{f}}{\partial x_j} + J_j^{SGS}\right], \tag{3}$$

where u_i is the i-th component of velocity, P is the pseudo-pressure $P = p - \frac{\rho}{3}\tau_k k$, f is the mixture fraction and ρ is the density. The subgrid term $J_j^{SGS} = \overline{f}\overline{u}_j - \overline{fu}_j$ is modelled using the gradient diffusion assumption

$$J_j^{SGS} = \overline{f}\overline{u}_j - \overline{fu}_j \approx \frac{\nu_t}{Sc_t}\frac{\partial \overline{f}}{\partial x_j}$$

Here ν_t is the so called turbulent viscosity. The unclosed stress tensor $\tau_{ij} = \overline{u_i u_j} - \overline{u}_i\overline{u}_j$ can be modeled in terms of filtered velocity $\overline{u}_i$ using the classical model proposed by Smagorinsky

$$\tau_{ij} = -2C_S\overline{\Delta}^2|\overline{S}|\overline{S}_{ij}. \tag{4}$$

where

$$\overline{S}_{ij} = \frac{1}{2}\left(\frac{\partial \overline{u}_i}{\partial x_j} + \frac{\partial \overline{u}_j}{\partial x_i}\right), \quad |\overline{S}| = (2S_{ij}S_{ij})^{1/2} \tag{5}$$

and C_S is a constant varying between 0.065 and 0.2 depending on the problem under consideration. The classical model of Smagorinsky suffers from certain drawbacks analysed e.g. in the review paper of Meneveau and Katz (2000). The important contribution to the improvement of the Smagorinsky model has been done by Germano (1991) who proposed the dynamic procedure (henceforth referred to as the DGM model) to calculate the model coefficient C_S. The models based on the eddy-viscosity formulation (4) overestimate the energy dissipation and are not able to consider the effects of the energy backscatter (Meneveu and Katz, 2000). To overcome these disadvantages Bardina et al. (1980) developed a family of models using the scale similarity hypothesis. These models capture anisotropic effects, energy backscatter and disequilibrium, but underestimate the energy dissipation. The mixed models based on the combination of the eddy-viscosity model and the similarity model have been derived to utilize the strengths of both models. One of the most popular mixed models was formulated by Zang et al. (1993) and improved by Vreman et al. (1994) (henceforth referred as DMM model)

$$\tau_{ij}^a = (\overline{\overline{u}_i\overline{u}_j} - \overline{\overline{u}}_i\overline{\overline{u}}_j)^a - 2C_S\overline{\Delta}^2|\overline{S}|\overline{S}_{ij}. \tag{6}$$

The superscript "a" denotes the anisotropic part of the tensor. The first term on the right-hand side of (6) is the similarity model and the second part represents the model for the unresolved residual stress, adopting the Smagorinsky eddy-viscosity formulation. The constant C_S in (6) is calculated dynamically so that it is a function in space and time. Like in the Germano procedure, the calculation is based on the introduction of an additional explicit test filtering with the filter width $\hat{\overline{\Delta}} = \alpha\overline{\Delta}$ and $\alpha = 2$. The final formula for C_S is written in the form

$$C_S = \frac{\langle M_{ij}(L_{ij} - Hij)\rangle}{\langle M_{ij}M_{ij}\rangle}. \tag{7}$$

where

$$L_{ij} = \widehat{\overline{u}_i\overline{u}_j} - \widehat{\overline{u}}_i\widehat{\overline{u}}_j. \tag{8}$$

$$M_{ij} = -2\hat{\overline{\Delta}}^2\,\widehat{|\overline{S}|\overline{S}}_{ij} + 2\overline{\Delta}^2\widehat{|\overline{S}|\overline{S}}_{ij}. \tag{9}$$

$$H_{ij} = \widehat{\widehat{\overline{u}}_i\widehat{\overline{u}}_j} - \hat{\overline{u}}_i\hat{\overline{u}}_j - (\widehat{\overline{u}_i\overline{u}_j} - \widehat{\overline{u}}_i\widehat{\overline{u}}_j). \tag{10}$$

Unfortunately, the constant C_S computed from (7) can take on a very large magnitude and that leads typically to strong numerical instability. To stabilize calculations an addtional spatial averaging $< \ldots >$ of the numerator and denominator over a homogeneous direction is introduced in the formula (7). For the complex flows homogeneous direction does not exist and therefore the introduction of the additional averaging is very problematic for engineering applications.

Another way to prevent the instability is a simple clipping of the constant C_S. Various clipping procedures are widely used to ensure the numerical stability of calculations. We apply a clipping procedure to the dynamic model derived from a rigorous mathematical analysis based on Taylor series approximation. Applying the Taylor expansion for velocity u_i the filtering procedures are reduced to simple integrations that are performed analytically. Using the second-oder approximation the terms of the DMM model can be written in the asymptotic form:

$$L_{ij} = \widehat{\overline{u}_i\overline{u}_j} - \widehat{\overline{u}}_i\widehat{\overline{u}}_j = \frac{\overline{\Delta}^2}{3}\frac{\partial\overline{u}_i}{\partial x_k}\frac{\partial\overline{u}_j}{\partial x_k} + O(\overline{\Delta}^4), \tag{11}$$

$$L_{ij}^m = \overline{\overline{u}_i\overline{u}_j} - \overline{\overline{u}}_i\overline{\overline{u}}_j = \frac{\overline{\Delta}^2}{12}\frac{\partial\overline{u}_i}{\partial x_k}\frac{\partial\overline{u}_j}{\partial x_k} + O(\overline{\Delta}^4), \tag{12}$$

$$\widehat{L}_{ij}^m = \widehat{\overline{\overline{u}_i\overline{u}_j}} - \widehat{\overline{\overline{u}}_i\overline{\overline{u}}_j} = \frac{\overline{\Delta}^2}{12}\frac{\partial\overline{u}_i}{\partial x_k}\frac{\partial\overline{u}_j}{\partial x_k} + O(\overline{\Delta}^4), \tag{13}$$

$$L_{ij}^T = \widehat{\hat{\overline{u}}_i\hat{\overline{u}}_j} - \hat{\overline{\overline{u}}}_i\hat{\overline{\overline{u}}}_j = \frac{5\overline{\Delta}^2}{12}\frac{\partial\overline{u}_i}{\partial x_k}\frac{\partial\overline{u}_j}{\partial x_k} + O(\overline{\Delta}^4). \tag{14}$$

Neglecting the terms of the fourth order $\sim O(\overline{\Delta}^4)$ we obtain simple asymptotical estimations

$$L_{ij}^m \approx \frac{1}{4}L_{ij}, \quad L_{ij}^T \approx \frac{5}{4}L_{ij}, \quad \widehat{L}_{ij}^m \approx \frac{1}{4}L_{ij}. \tag{15}$$

Computational experience shows that the numerical instability is caused mostly by the term H_{ij}. The reason for that is probably the inaccuracy of the numerical triple filtering of the velocity field for calculation of terms $\widehat{\hat{\overline{u}}_i\hat{\overline{u}}_i}$ and $\hat{\overline{\overline{u}}}_i$. To restrict the tensor H_{ij} from above we apply a simple clipping procedure based on the estimations (15):

$$L_{ij}^T = \begin{cases} L_{ij}^T, & \text{if } L_{ij}^T \le \frac{5}{4}L_{ij} \\ \frac{5}{4}L_{ij}, & \text{else} \end{cases} \tag{16}$$

and

$$\widehat{L}_{ij}^m = \begin{cases} \widehat{L}_{ij}^m, & \text{if } \widehat{L}_{ij}^m \le \frac{1}{4}L_{ij} \\ \frac{1}{4}L_{ij}, & \text{else} \end{cases} \tag{17}$$

An important advantage of the restrictions (16) and (17) is that the tensors L_{ij}^T and $\widehat{L}_{ij}^m$ are compared with the tensor L_{ij} which is anyway calculated for the estimation of the constant C_S (7). No additional calculations are required for the clipping procedure. Additionally to clipping (16) and (17) we set C_S to be zero when it becomes negative to prevent the appearance of negative turbulent viscosity.

Simulation of spatially inhomogeneous turbulent flows using LES requires specification of unsteady turbulent inlet boundary conditions. Therefore we developed a novel inflow generation technique (Kornev, 2003) which allows us to generate turbulent inlet velocities with prescribed autocorrelation functions and integral length scales taken from auxiliary LES calculations. The idea is based on a random placing fictitious turbulent spots characterized by a random sign, size and distribution of velocity within the spot. The algorithm generates a signal with prescribed spatial integral length scales, integral time scales, two-point spatial and one point temporal autocorrelations, as well as one-point cross correlations between fluctuation components.

EXPERIMENTAL SETUP

for the complex flows Experiments were made in the closed water pipe (Fig.2). Water from tanks 1 and 2 is pumped by pump 3 into intermediate tank 4 and via steel tube 5 of 50 mm inner diameter and of 5000 mm length flows to measuring section 7 via intermediate block 6. Measuring section 7 of the pipe made of perspex, is 1000 mm long and comprises rectangular box 8 in which 50 mm inner diameter tube 9 is mounted. Box 8 is filled with water to reduce the optical distortion of a test flow volume due to the tube curvature. Tube 9 is connected with intermediate block 6 in which tube 10 (nozzle) is mounted co-axially with the axes of tubes 5 and 9. The length of the horizontal section of tube 10 is no less than its 50 diameters. Tubes 9 and 10 form a co-axial mixer.

A weak 0.03 mg/l aqueous rhodamine solution 6G is injected through nozzle 10 via pump 11 from tank 12. The mixed medium after the mixer enters tanks 13 and 14, in order to keep the initial radiation intensity level over the entire time of measurement. Flow rate meters 15 control flowrates of media in each of the supplied lines within the accuracy of ± 1 per cent. Heater 16 mounted on steel tube 5 varies the temperature of water that enters the mixer.

Passive admixture fields were measured using the LIF method. A beam of a pulsed $Nd:YAG$ laser with a wavelength of 532 nm and a pulse duration of 7 ns is transformed by means of cylindrical and two spherical lenses to a laser sheet 0.8 mm thick. This sheet oriented along the mixer axis in the vertical plane excites rhodamin molecules. In going to the normal state, the excited molecules emit longer waves that pass through a filter to an objective of the CCD camera (PI-MAX, Roper Scien. Corp). In that case when the effect of light absorption by rhodamine molecules can be neglected, there exists a simple relationship $I = kC$ between the emitted rhodamine intensity I and the rhodamine concentration C. The linear dependency is hold at a realatively small power of a laser beam (no more than 400 mW) and weak aqueous rhodamine solution concentrations not exceeding 0.08 mg/l. These conditions are completely fulfilled in this research.

A laser served as an outer trigger for the camera. The spatial resolution of the experiment is estimated as ~ 0.3 mm. The time resolution is limited by the maximum frequency of laser pulsations that was only 10 Hz. Passive scalar distributions over the mixer cross sections is calculated from the intensity distributions I referred to the maximum intensity I_0 in the first cross section.

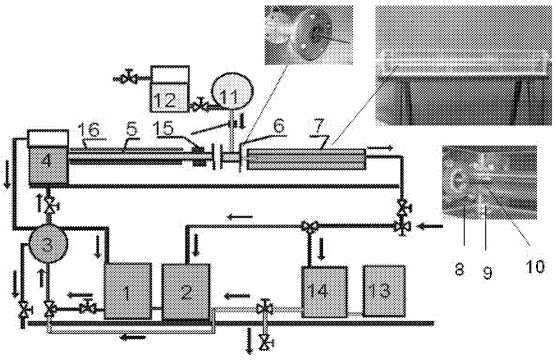

Figure 2: Experimental set-up

RESULTS

Numerical calculations are carried out in the computational domain with the length of eight diameters of the pipe using an inhouse code for LES and the commercial code CFX for RANS. In terms of D the computational domain has the size $8 \times 1 \times 2\pi$ in a cylindrical coordinate system (x, θ, r). The grid contains $N_x \times N_\theta \times N_D$ cells in axial, circumferential, radial directions of the pipe and N_d in radial direction of the nozzle. Test calculations with three following grids $N_x = 128$, $N_\theta = 32$, $N_D = 8$, $N_d = 2$; $N_x = 256$, $N_\theta = 64$, $N_D = 16$, $N_d = 3$; and $N_x = 512$, $N_\theta = 64$, $N_D = 32$, $N_d = 6$ shown that the difference between two last grids is insignificant. To save the computational time only the second grid was used for calculations. The grid is nearly equidistant in x and r directions and provides almost cubical cells at $r/D = 0.6$ what is in agreement with requirements formulated in Forkel (1999) for pipe flows.

Influence of different parameters on mixing

Table 1 summarizes numerical and experimental investigations of the influence of different parameters on the overall mixing obtained in Jahnke, 2004 and Hassel, 2005 for both flow regimes mentioned in the Introduction. Parameter α is the degree of mixedness written in the form (see (Danckwerts, 1952))

$$\alpha = 1 - \frac{\int_S (f(x,r,\theta) - f_{av}(x))^2 dS}{\int_S (f(0,r,\theta) - f_{av}(0))^2 dS},$$

where $f_{av}(x) = \frac{1}{S}\int_S (f(x,r,\theta)dS$, S is the area of the cross-section of the jet mixer. The mixing length $l_{0.9}$ is defined as the length at which the parameter α attains the value 0.9. Symbols in the Table 1 characterize the influence of the increase of different parameters on the mixing: 0- negligible influence, + weak enhancement, ++ strong enahncement of the mixing. The symbol NI stands for "not investigated". The most effect on the mixing has the flow rate ratio $\dot{V}_d/\dot{V}_D$. As seen from the Table 1 the flow and mixing can be positevely affected by the two following methods of flow control

- swirling the jet $\Omega = \omega d/U_d$, where ω is the angular velocity, and
- flow rate oscillations $\dot{V}_d/\dot{V}_D = C(1 + A\sin\frac{2\pi U_d Sh}{d}t)$, where A is the magnitude and Sh is the Strouhal number of oscillations. If the excitation frequency is close to the natural frequencies of the vortices generated between the jet and the coflow we have an effect similar to resonance that is in this case for Strouhal numbers between 0.2 and 0.4. The mixing length can be reduced by 25 per cent in the resonance case.

Flow structures in the jet mixer

One of the ways to understand the nature of mixing is the investigation of the development of vortex structures. For this aim the vortex identification method based on the λ_2 criterion proposed by Jeong and Hussain (Jeong, 1995) has been used. This analysis shows that there are no dominant regular vortex structures in the mixer flow. Particularly, the vortex structures, identified as the iso-surfaces $\lambda_2 = -4 \cdot 10^4$ look like a tree with branches oriented against the flow (Fig. 3). Topologically similar structures were observed by LIF visualizations of the scalar field. Weak coherent vortex structures are revealed near the wall (see Fig. 4). They are responsible for the positive or negative sign of the autocorrelation function at $r/D = -0.28$ and $r/D = 0.34$ in the area of the recirculation zone $x/D \approx 1.7$ (see Fig. 5). Analysis of vortex lines of the vorticity field shows that the at small distances $x/d < 3$ the vortex lines are regular rings which then experience azimutal instability transforming into crude irregular structures.

Comparative study of scalar mixing using different RANS and LES models

The flow in the jet mixer was calculated using dynamic mixed model with random inlet conditions (DMM random), dynamic Germano model (DGM) and classical Smagorinsky model. For comparison the calculations were performed with SST, $k-\epsilon$ and RSM models of RANS. Since the regime with

Table 1: Influence of different parameters on mixing enhancement

Parameter	numerical simulation			LIF		
	range	Influence on α	Influence on $l_{0.9}$	range	Influence on α	Influence on $l_{0.9}$
$\dot{V}_d/\dot{V}_D$	0.18-0.6	++	++	0.2-0.769	++	++
Re_d	$5 \cdot 10^3 - 1.6 \cdot 10^5$	at $x/D < 6$	0	$10^4 - 1.5 \cdot 10^4$	0	0
ρ_d/ρ_D	0.6-1.6	at $x/D < 3$	0	NI	NI	NI
Sc	0.7-1000	0	0	NI	NI	NI
$\frac{\lvert T_D - T_d \rvert}{T_D}$	0-0.229	0	0	0-0.12	0	0
Swirling	Ω=0-1.1	++	++	NI	NI	NI
var $\dot{V}_d/\dot{V}_D$	$Sh = 0...3$	++	++	NI	NI	NI
	$A = 0...1$					

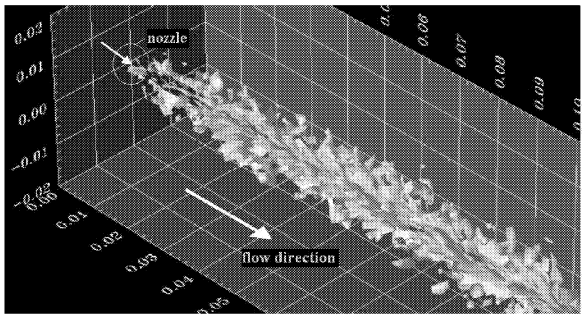

Figure 3: Vortex structures of the flow identified as the iso-surfaces $\lambda_2 = -4 \cdot 10^4$. $Re_d = 10^4, Re_D = 2800$, $\dot{V}_D/\dot{V}_d = 1.3$, $D/d = 5$, LES calculation

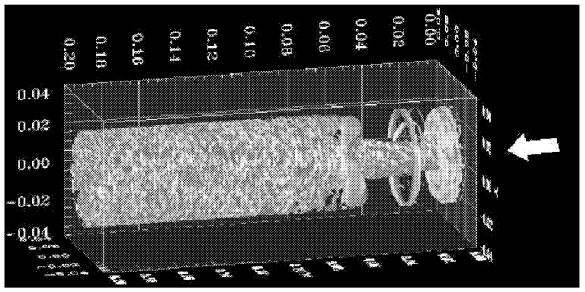

Figure 4: Wall vortex structures of the flow identified as the iso-surfaces $\lambda_2 = -10^{-2}$. $Re_d = 10^4, Re_D = 2800$, $\dot{V}_D/\dot{V}_d = 1.3$, $D/d = 5$, LES calculation

the recirculation zone is the most difficult from the hydrodynmic point of view the results are presented only for this regime.

The measurements show that the time averaged flow is not axisymmetric especially in the area of the recirculation zone. At present it is still not quite clear what is the reason of this asymmetry. Perhaps, this is a result of small errors of the set-up installation although deviations between the axis of the intermediate block 6 and the measuring section 7 were less than ~ 0.5 mm. So, at present we do not exclude physical reasons of this effect. An asymmetry is observed to a certain extent in calculations and depends on the interval of the time averaging. This phenomenon is the subject of our future research. The comparison between the theory and measurements suffers from some drawbacks because the LIF measurements deliver data only in one plane. To take into account the asymmetry effect the intermediate block 6 with the nozzle was rotated around the axis. The maximum difference for the scalar distribution is obseverd for two positions of the nozzle at circumferential coordinates $\theta = 0^o$ and $\theta = 180^o$. The experimental data for these two positions were used further for comparisons.

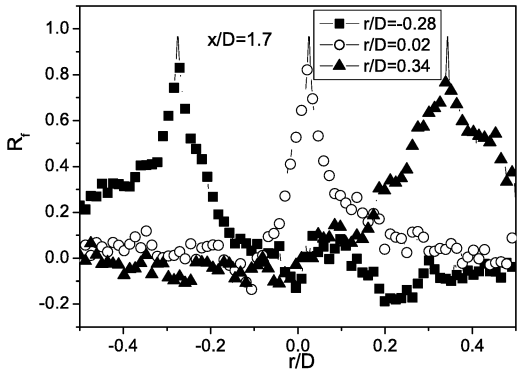

Figure 5: The two-point auto correlation $R_f(r,\eta) = \overline{f'(r)f'(r+\eta)}/(\sqrt{\overline{f'^2(r)}}\sqrt{\overline{f'^2(r+\eta)}})$ across the mixer in the cross-section $x/D = 1.7$. $Re_d = 10^4, Re_D = 2800$, $\dot{V}_D/\dot{V}_d = 1.3$, $D/d = 5$, LIF measurement

The SST model shows a very good agreement with measurements for the flow regime with the recirculation zone (Fig. 6). It confirms the well known opinion that the SST model is very robust for separating flows. The accuracy of the $k-\epsilon$ and RSM RANS models is worse than that of the SST model and DMM LES simulations. Unexpectedly, the Germano model (DGM) shows a very poor capability to predict the mixing for all x/D. Many efforts to improve the prediction were implemented. The changing inlet conditions, increasing the resolution, artificial inclination of the nozzle jet, local grid refinement, enlargement of the computational domain by including a part of the nozzle and implementation of different wall functions have not led to any success. The discrepancy between DGM calculations and measurement is extremely large at $r/D > 0.2$ within the length $1.0 < x/D < 1.5$. In this region the Germano model shows no admixture $f = 0$ what contradicts the measurements and results obtained with other RANS and LES models. Bearing in mind that the scatter of experimental data in region $r/D > 0.2$ and $1.0 < x/D < 1.5$

is about 0.1 we can conclude that the accuracy of prediction using the DMM model and SST RANS model is quite good. The results of the Smagorinsky model are strongly dependent on the value of the constant. By variation of the constant it is possible to get a number of different solutions. Taking C being equal to 0.065 we get the solution, which is close to the DGM solution. The use of common values $C = 0.1$ and $C = 0.17$ results in an extremely delayed mixing.

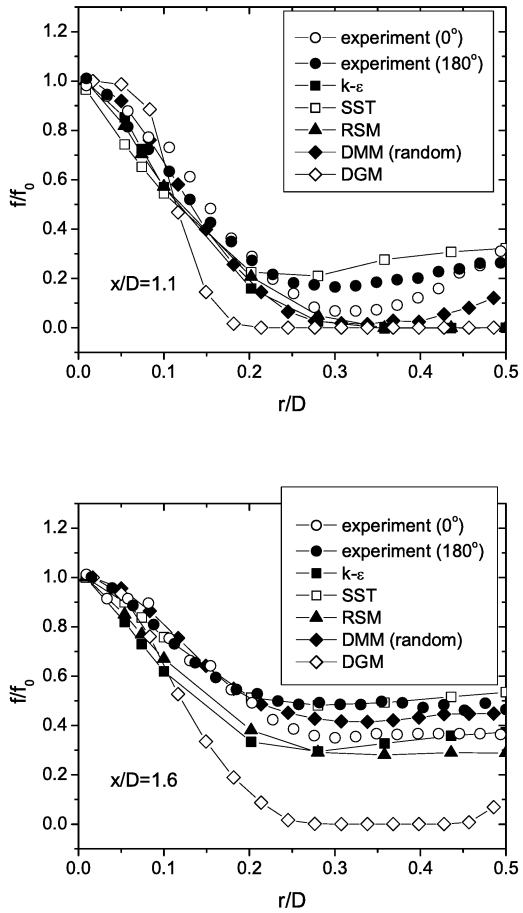

Figure 6: The mean profiles of the mixture fraction in sections $x/D = 1.1$ and $x/D = 1.6$. $Re_d = 10^4, Re_D = 2800$, $\dot{V}_D/\dot{V}_d = 1.3$, $D/d = 5$

Snapshots of the mixture fraction show that the jet is "destroyed" faster when the DMM model is applied. There are two reasons for that. Firstly, the turbulent viscosity and the dissipation term of the DMM model $-2C_S\overline{\Delta}^2|\overline{S}|\overline{S}_{ij}$ are much less than those of the DGM model for small $x/D < 2.0$ (see Fig. 7). On the contrary, the SGS stresses of the DMM calculation are larger (Fig. 8) in the initial area of the jet development. At $x/D > 2.0$ the situation changes as the vortices in the DMM calculation are weakened, whereas the vortices of the DGM calculation only come into play. Secondly, due to the presence of the first term $(\overline{\overline{u}_i\overline{u}_j} - \overline{\overline{u}}_i\overline{\overline{u}}_j)^a$ the DMM model is able to capture the energy backscatter which is very strong in the area of the jet boundaries again in the initial part of the jet. Both effects lead to stronger vortex structures and enhance mixing.

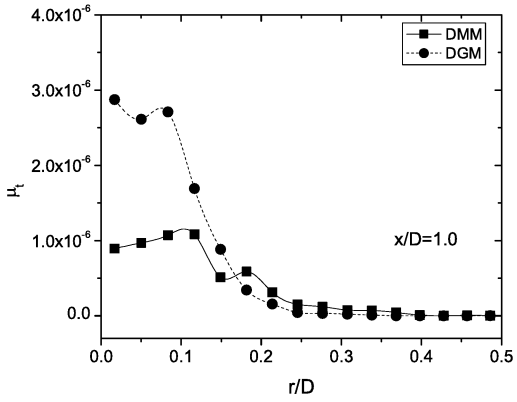

Figure 7: The profiles of the turbulent viscosity in the section $x/D = 1.0$. $Re_d = 10^4, Re_D = 2800$, $\dot{V}_D/\dot{V}_d = 1.3$, $D/d = 5$

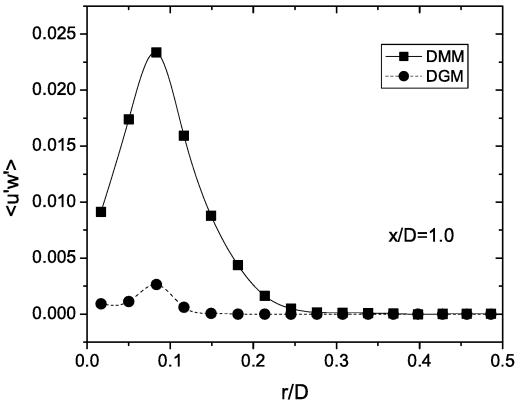

Figure 8: The profiles of the stress $< u'w' >$ in the section $x/D = 1.0$. $Re_d = 10^4, Re_D = 2800$, $\dot{V}_D/\dot{V}_d = 1.3$, $D/d = 5$

Bearing in mind analysis published in Pope (2004) we can not claim that one SGS model is principially worse than the other. Indeed, as shown in Pope (2004) the DGM and the Smagorinsky model must lead to identical results when the resolution is good enough and the modelled subgrid scales are in the inertial subrange. On the basis of the present analysis we can only conclude that the DMM model is more accurate than the DGM model for the resolution used in this paper.

Influence of the inflow boundary conditions

The influence of the inflow generator proposed by Kornev (2003) is illustrated in Fig. 9. Qualitatively, the mixing with the inflow generator occurs faster than that with random inlet conditions. For large x/D it is difficult to draw any consequences since both curves fall within the scatter predicted by measurements. Advantages of the inflow generator are seen at small $x/D = 1.1$ The numerical simulation becomes more accurate at $r/D > 0.3$. Most serious advantages of the realistic inlet conditions become clear when the resolution increases. Vorticities of the random inlet velocity field decrease with increasing resolution. Indeed, the length scales of the

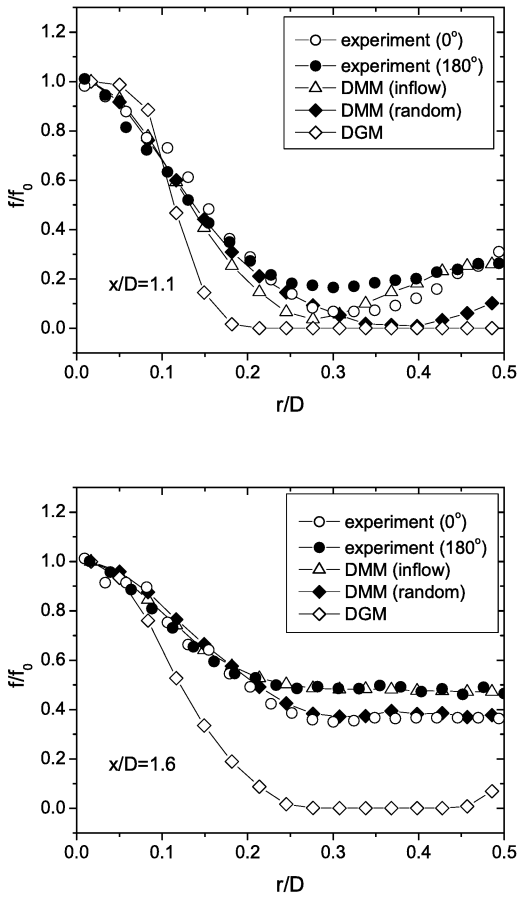

Figure 9: Influence of the inlet boundary conditions. The mean profiles of the mixture fraction in sections $x/D = 1.1$ and $x/D = 1.6$. $Re_d = 10^4, Re_D = 2800$, $\dot{V}_D/\dot{V}_d = 1.3$, $D/d = 5$.

random inlet signal are proportional to the size of grid cells. The results are strongly dependent on the resolution. On the contrary, the application of the inflow generator reduces the influence of the resolution on numerical results because the integral length scales of the inflow velocity field are independent of cell sizes. In this case the difference between solutions for the grid used $N_x = 256$, $N_\theta = 64$, $N_D = 16$, $N_d = 3$ and the finer one $N_x = 512$, $N_\theta = 64$, $N_D = 32$, $N_d = 6$ is insignificant.

CONCLUSIONS

Flow phenomena in a coaxial jet mixer are studied using numerical (LES) and experimental (LIF) methods. A simple clipping procedure derived by the authors from a rigorous mathematical analysis and a novel inflow generator for turbulent inlet boundary conditions were succesfully implemented. As shown both theoretically and experimentally the most effect on the mixing have the flow rate ratio $\dot{V}_d/\dot{V}_D$ and the diameter ratio D/d whereas the influence of other parameters is negligible in the investigated range of their variations. The mixing can be essentially enhanced by two methods of flow controls: flow rate oscillations with excitation frequences close to the natural frequences of vortices generated behind the nozzle and jet swirling. The analysis of flow structures revealed no dominant regular vortex structures. However, weak coherent vortex structures are revealed close to the wall. Application of the inflow generator with prescribed integral length scales results in the two following effects: the solution becomes less sensitive to the resolution and the mixing occurs faster compared with the numerical solutions using random inlet conditions. Comparative study using several RANS and LES models show that the dynamic mixed SGS model of LES and SST model of RANS provides the best accuracy of mixing prediction in the flow with the recirculation zone.

ACKKNOWLEDGEMENT

The study was supported by the Deutsche Forschungsgemeinschaft within framework of the program SPP 1141.

REFERENCES

Barchilon M., Curtet R., "Some details of the structure of an ussymetric confined jet with backflow." *J. Basic Engineering*, 1964, pp. 777-787.

Bardina J. J., Ferziger H., Reynolds W. C., "Improved subgrid models for large eddy simulation." *AIAA Paper 80-1357* 1980.

Danckwerts P.V., "The definition and measurement of some characteristics of mixtures." *Appl. Sci. Res., Sect. A3* 1952, pp. 279-296.

Forkel H., "Ueber die Grobstruktursimulation turbulenter Wasserstoffdiffusionsflammen." *Fortschritt-Berichte VDI* 1999, Nr.428, P.152.

Hassel E., Jahnke S., Kornev N., Tkatchenko I., and Zhdanov "Numerical and experimental study of turbulent processes and mixing in jet mixers." *ERCOFTAC Symposium -ETMM6*, Sardinia, Italy, 23-25 May, 2005, accepted for publication.

Henzler H.J., "Investigations on mixing fluids." *Dissertation* 1978, RWTH Aachen, P.60.

Jahnke S., Kornev N., Tkatchenko I., Hassel E., Leder A., "Numerical study of influence of different parameters on mixing in a coaxial jet mixer using LES." *Heat and Mass Transfer* 2004, **DOI**:10.1007/s00231-004-0521-9.

Jeong J., Hussain F."On the identification of a vortex." *J.Fluid Mech.* 1995, vol.285, pp. 69-94.

Kornev N., Hassel E., "A new method for generation of artificial turbulent inflow data with prescribed statistic properties for LES and DNS simulations." *Schiffbauforschung* 2003, Vol.42, pp. 35-44 (is prepared for submission to J.Comput.Physics).

Meneveau C., Katz J.,"Scale-invariance and turbulence models for large-eddy simulation." *Annu. Rev. Fluid Mech.* 2000, Vol.32, pp. 1-32.

Pope S., "Ten questions concerning the large-eddy simulation of turbulent flows." *New Journal of Physics* 2004, Vol. 6(35),**DOI**:10.1088/1367-2630/6/1/035.

Vreman B., Geurts B., Kuerten H., "On the formulation of the dynamic mixed subgrid-scale model." *Physics Fluids* 1994, Vol. 6(12), pp. 4057-4059.

Zang Y., Street R. L., Koseff J. R., "A dynamic mixed subgrid-scale model and its application to turbulent recirculating flow." *Physics Fluids* 1993, Vol. A5(12), pp. 3186-3196.